論文98-35S-7-7

대규모 위상배열용 적응 빔 형성 알고리듬의 성능비교

(Performance Comparisons of Adaptive Beamforming Algorithms for a Large Distorted Phased Array)

姜 鳳 淳 *, 朴 成 鈞 **

(Bong-Soon Kang and Seong-Gyoon Park)

요 약

본 논문은 대규모 위상배열용 최적의 적응 빔 형성(adaptive beamforming: ABF) 알고리듬을 선택하는 기준에 대한 실험적 증명을 제시한다. Clutter에 둘러싸인 single point target 모델을 사용하여, 네 가지의 잘 알려진 적응 빔 형성 알고리듬들을 비교한다. 거대한 위상어레이를 자체교정하기 위하여 사용되는 이 알고리듬들은 작은 분산과 큰 분산의 특성을 보유하고 있는 실제 데이터를 사용하여 검증한다. 이 알고리듬들은 실험대상 영역에 적어도 한 개의 큰 반사능력을 가진 scatterer나 다소 반사능력 떨어지는 몇 개의 scatterer들을 필요로 한다. 실험 데이터에서 복원된 cross-range 이미지, range-azimuth 이미지와 더불어 gain loss, 이미지 상관계수를 사용하여 네 가지 알고리듬들을 비교 분석한다.

Abstract

This paper presents an experimental proof for criteria of selecting an optimum adaptive beamforming (ABF) algorithm for a large distorted phased array. A single point target embedded in clutter model is suggested to compare four well-known ABF algorithms. These algorithms are tested to low variance and high variance real data for self-calibrating a large distorted phased array. It is shown that these algorithms require at least one dominant scatterer with large radar cross section (RCS) or multiple scatterers with moderate RCS in the field of view. Experimental results are provided to demonstrate the comparisons of the four algorithms in terms of gain loss and image correlation coefficient, along with corresponding reconstructed cross-range images and range-azimuth images.

I. Introduction

A microwave radar imaging system has beenintroduced in the literature as a "radio camera" capable of "taking pictures" of microwave scattering objects with an angular resolving power as high as 10^{-4}-10^{-5} rad, which is typical of common optical instruments such as cameras and small telescopes[1]. The radio camera is a high resolution, two-dimensional microwave imaging instrument in which the distortion in its large aperture, which is usually a large phased array, is self-corrected by a process called ABF. Its success depends upon the known properties of the reradiation from a target or

* 正會員, System LSI, 三星電子
(System LSI, Samsung Electronics Co.)
** 正會員, 公州大學校 情報通信學科
(Dept. of Information & Communication Eng., Kongju National University)
接受日字:1997年6月10日, 수정완료일:1998年6月12日

scatterer having large radar cross section and small physical size[2],[3]. The aforementioned self-cohering procedure is called the dominant scatterer algorithm (DSA)[4]. A modified algorithm, suggested by Attia, is described in[5]. It synthesizes a beamforming source when no satisfactory one exists. It is called the multiple scatterer algorithm (MSA)[6]. An even higher quality image can be obtained when subarray processing is added to the MSA method. According to whether there exists overlapping between adjacent subarrays, the modified procedure is called the multiple scatterer algorithm with nonoverlapping subarray processing (MSA-S) or the multiple scatterer algorithm with overlapping subarray processing (MSA-OS)[7]. The above-mentioned dominant scatterer class of algorithms requires at least one dominant scatterer or multiple scatterers in the field of view.

In this paper, we develop a model of a single point target embedded in clutter and derive the condition for a point scatterer to be eligible for a beamformer (Section 2). In Section 3, we describe two well-known measures of beamformer quality. Experimental results are followed in Section 4 where two measures and reconstructed images obtained after selfcalibrating a distorted phased arrays with the four algorithms are compared.

II. Single Point Target Embedded in Clutter Model

The reradiating signal from a point source illuminates the received phased array with a spherical wavefront. The complex field amplitude (CFA) at some instant of time in the nth receiving channel can be written as

$$e(x_n) = a_n e^{j\phi_n} \tag{1}$$

where a_n and ϕ_n are amplitude and phase, respectively. In a large distorted array, the amplitude from such a point target will be constant approximately across the array ($a_n = a$), whereas the phase is random from antenna element to element because of the geometric distortion in the aperture. It is assumed that the phase can be modeled as a random variable having uniform distribution over $[-\pi, \pi]$.

In real microwave imaging situations, such a point target is usually embedded in clutter. Figure 1 illustrates a point target embedded in clutter. Assuming that the clutter consists of a large number of independent scatterers, the CFA measured at the nth receiver can be written as the sum

$$e(x_n) = ae^{j\phi_n} + c_n e^{j\delta\phi_n} \tag{2}$$

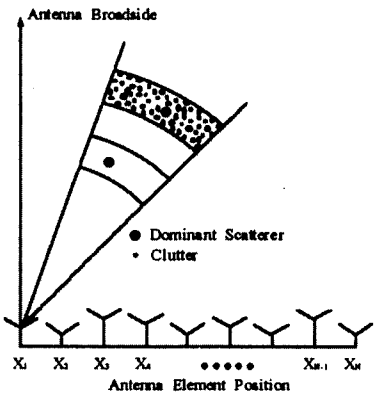

그림 1. Clutter에 둘러싸인 single point target
Fig. 1. Single point target embedded in clutter.

where c_n and $\delta\phi_n$ are the amplitude and the phase caused by the clutter, respectively. Assume that ϕ_n and $\delta\phi_n$ are uncorrelated. Provided that the targ ($a^2 \gg c_n^2$)et strength is superior to the clutter strength , the magnitude of the CFA and its expected value are

$$|e(x_n)| = \sqrt{a^2 + c_n^2 + 2ac_n\cos(\phi_n - \delta\phi_n)}$$

$$\approx a\left(1 + \frac{c_n^2}{2a^2} + \frac{c_n}{a}\cos(\phi_n - \delta\phi_n)\right.$$

$$-\frac{c_n^2}{2a^2}\cos 2(\phi_n-\delta\phi_n)\}$$

$$= a\{1+\frac{c_n^2}{4a^2}+\frac{c_n}{a}\cos(\phi_n-\delta\phi_n)$$

$$-\frac{c_n^2}{2a^2}\cos 2(\phi_n-\delta\phi_n)\} \quad (3)$$

$$E[|e(x_n)|] = a\{1+\frac{E[c_n^2]}{4a^2}\} \quad (4)$$

where $(1+x)^{1/2}=1+x/2-x^2/8+\cdots$ with $x \ll 1$, $\cos^2\phi=(\cos 2\phi+1)/2$ and $E[\cos 2(\phi_n-\delta\phi_n)]=0$. $|\ |$ denotes absolute value. The expected value of the magnitude is not equal to a because of the bias due to the clutter. The expected value of the square magnitude of the CFA is

$$E[|e(x_n)|^2]=E[e(x_n)e^*(x_n)]=a^2+E[c_n^2] \quad (5)$$

where * denotes complex conjugation. From (4) and (5), we get

$$a=\frac{2}{3}E[|e(x_n)|]\{1\pm\sqrt{1-\frac{3E[|e(x_n)|^2]}{4(E[|e(x_n)|])^2}}\}. \quad (6)$$

For simplicity, $(E[\ ])^2$ will hereafter be denoted as $E^2[\ ]$. Since the measured amplitude a is real, the inside square term should be greater than or equal to zero. Thereby, we get

$$\frac{E^2[|e(x_n)|]}{E[|e(x_n)|^2]} \geq \frac{3}{4}. \quad (7)$$

The amplitude variance σ_A^2 of the measured echoes in the aperture domain is

$$\sigma_A^2=E[|e(x_n)|^2]-E^2[|e(x_n)|]. \quad (8)$$

The amplitude variance normalized to the expected value of the square magnitude is

$$\sigma_{NA}^2=\frac{\sigma_A^2}{E[|e(x_n)|^2]}=1-\frac{E^2[|e(x_n)|]}{E[|e(x_n)|^2]}. \quad (9)$$

Using the inequality condition of $E^2[|e(x_n)|]/E[|e(x_n)|^2]\geq 3/4$ in (9) gives

$$\sigma_{NA}^2 \leq \frac{1}{4}. \quad (10)$$

This inequality implies that the model of a single point target embedded in clutter is applicable to the normalized amplitude variance of 0.25 or less. Therefore, this value is the largest amplitude variance that the dominant scatterer class of algorithms can be used for the ABF. An approach for ABF under the high variance condition was suggested in [8] by averaging complex field amplitude (CFA) across multiple range bins. It decorrelated coherence properties of microwave measurements by spatially smoothing the received CFA.

Ⅲ. Measures of Beamformer Quality

The phase errors, which remain even after compensating the array weight vector in antenna aperture domain through the ABF algorithms, affect the degradation in image quality [6]. Hence, it can be said that the amount of the phase errors determines the performance of ABF algorithms. To evaluate their performance, rather than directly examining the phase-error variance, two measures of gain loss and correlation are generally used. The actual main-beam gain relative to the errorfree main-beam, which is the fractional loss in gain, is given by the tolerance theory [4]. The gain loss in decibels, called $\triangle G$, is

$$\triangle G = 4.34\ \sigma_{\delta\phi}^2. \quad (11)$$

where $\sigma_{\delta\phi}^2$ denotes phase-error variance across the array.

An image correlation measure has proved useful in comparing two microwave images [9]. The correlation ρ between two images is

$$\rho=\frac{E[\int_{-1}^{1}|\hat{S}_1(u)\ \hat{S}_2^*(u)|du]}{\sqrt{E[\int_{-1}^{1}|\hat{S}_1(u)|^2du]E[\int_{-1}^{1}|\hat{S}_2(u)|^2du]}} \quad (12)$$

where $\hat{S}_1(u)$ is the error-free image and $\hat{S}_2(u)$ is the image produced by an aberrated system.

Ⅳ. Experimental Results

The 83-m, 330-element quasi-linear array operating at 9.6 GHz, having 3-m range resolution and 2-m cross-range resolution, and producing 75 range bins, was used to image the nuclear power plant in Limerick, PA, USA, located 17.6 km from the array [4]. A basic ABF algorithm for self-calibrating a distorted phased array is called the DSA. It requires a single point target having large RCS or source strength in the field of view. This target always produces an image correlation of 0.9 or higher [10]. Beamforming bins having the normalized amplitude variances not larger than 0.12 have been shown to yield satisfactory images when the DSA is used for phase-cohering an array [11]. The four algorithms discussed in this paper were implemented by Fortran program. By using the program with the experimental data, a comparison was made using low variance range bins ($\sigma_{NA}^2 \leq 0.12$). A range bin containing a specular-like beamformer of amplitude variance of 0.06 is selected as an adaptive beamformer for the DSA. This range bin is bin 67. Bins 29 and 32 are used as candidate bins for the MSA class of algorithms. Their σ_{NA}^2 are 0.07, and 0.09, respectively. A second comparison was made using low quality range bins ($0.12 < \sigma_{NA}^2 \leq 0.25$), none of which was favorable for imaging. These range bins were bins 17, 25, and 26 having σ_{NA}^2 of 0.20, 0.21, and 0.23, respectively.

All these results are also compared by using image correlation coefficient in (12). The MSA-OS image under low variance condition is used as the reference image to calculate the coefficient.

1. Experiments under low variance condition ($\sigma_{NA}^2 \leq 0.12$)

Figure 2 shows 1-D cross-range images of bin 32 under low variance condition. The dotted line, which is 25 dB below the peak, is a typical threshold value below which signals are not displayed in 2-D range-azimuth imagery. It is close to the average sidelobe level (ASL) of 10 *log* (1/N), where N is the number of antenna array elements. Bin 32 falls in a high cooling stack in the Limerick nuclear power plant.

Figure 2a shows the performance of DSA. The measured maximum amplitude is 62.05 in amplitude units. The peak sidelobe level (PSL) is -11.1 dB. The resulting root mean square (*rms*) phase error is 23.57° and the corresponding gain loss is 0.73 dB. Figure 2b shows the performance of MSA using high quality bins 29, 32, and 67. The maximum amplitude and the PSL are 65.61 and -14.6 dB, respectively. The *rms* phase error and the gain loss are 10.07° and 0.13 dB. Figure 2c shows the performance of MSA-S. The entire array was divided into three identical subarrays, each containing 110 elements. The measured values are 65.24, -15.5, 9.45, and 0.12, respectively. Figure 2d shows the performance of MSA-OS. The entire array was divided into two 113-element subarrays and one 119-element subarray having 8 overlapped elements between adjacent subarrays. The measured values are 64.66, -12.0, 9.38, and 0.12, respectively. All these experimental results are listed in Table 1.

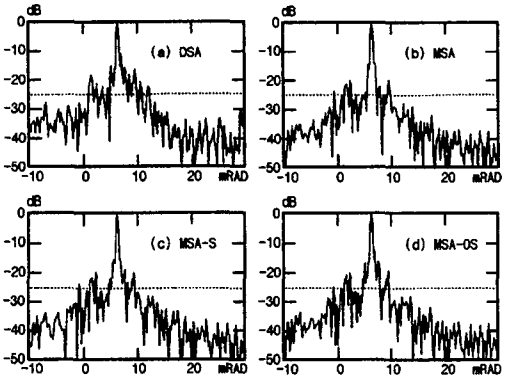

그림 2. 작은 분산 조건하에서 얻어진 bin 32의 cross-range 이미지 (a) DSA, (b) MSA, (c) MSA-S, (d) MSA-OS

Fig. 2. Cross-range images of bin 32 under low variance condition. (a) DSA, (b) MSA, (c) MSA-S, (d) MSA-OS

표 1. 작은 분산 조건하에서의 dominant scatterer류의 알고리듬의 비교
Table 1. Comparison of dominant scatterer class of algorithms under low variance condition.

ABF Algorithm	DSA	MSA	MSA-S	MSA-OS
Figure 2	a	b	c	d
σ^2_{NA} of bins	0.06 - -	0.06 0.07 0.09	0.06 0.07 0.09	0.06 0.07 0.09
Max amplitude	62.05	65.61	65.24	64.66
PSL (dB)	-11.1	-14.6	-15.5	-12.0
rms phase errors in degrees	23.57	10.07	9.45	9.38
ΔG (dB)	0.73	0.13	0.12	0.12

Figure 3 shows 2-D range-azimuth images of the power plant. Although the MSA class of algorithms reduces the phase errors and thereby produces an improved image, the DSA image of Figure 3a is of a sufficient quality so that the use of the MSA algorithms is not justified.

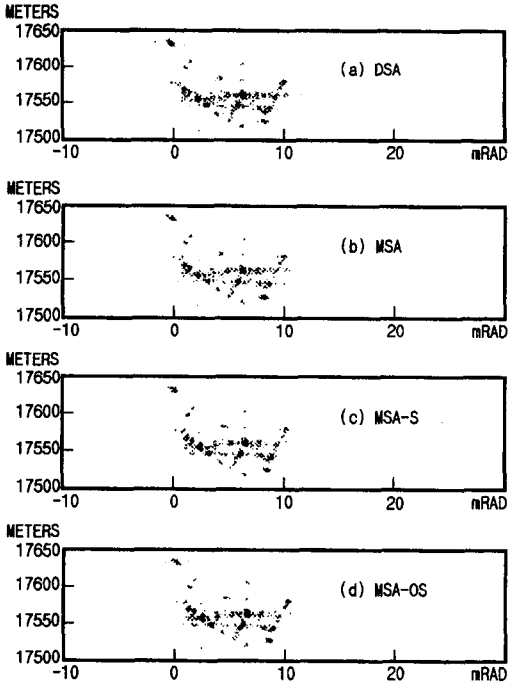

그림 3. 작은 분산 조건하에서 얻어진 Limerick 핵발전소의 range-azimuth 이미지 (a) DSA, (b) MSA, (c) MSA-S, (d) MSA-OS
Fig. 3. Range-azimuth images of Limerick nuclear power plant under low variance condition. (a) DSA, (b) MSA, (c) MSA-S, (d) MSA-OS

2. Experiments under high variance condition ($0.12 < \sigma^2_{NA} \leq 0.25$)

Figure 4 shows the cross-range images of bin 32 under high variance condition. Figure 4a shows the performance of DSA with bin 26 as the reference ABF bin. The measured maximum amplitude is decreased to 51.08 and the PSL has risen to -6.9 dB. The *rms* phase error is now increased to 46.74° and the corresponding gain loss is increased to 2.89 dB. Thus, many sidelobes rise above the threshold.

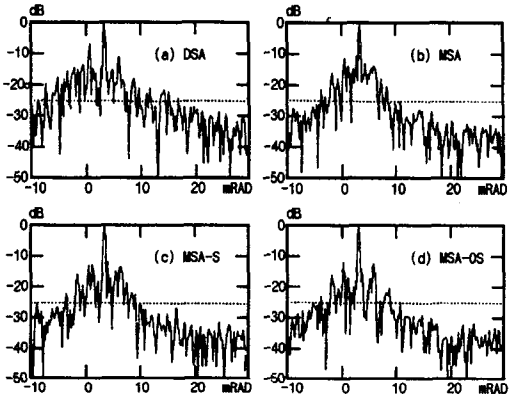

그림 4. 큰 분산 조건하에서 얻어진 bin 32의 cross-range 이미지 (a) DSA, (b) MSA, (c) MSA-S, (d) MSA-OS
Fig. 4. Cross-range images of bin 32 under high variance condition. (a) DSA, (b) MSA, (c) MSA-S, (d) MSA-OS

This experiment demonstrates that bin 26, whose σ^2_{NA} is 0.23, is a very poor beamformer for the DSA. Figure 4b shows the performance of MSA. Although bin 26 produces a useless image, the MSA performs quite satisfactorily when additional candidate beamforming bins of equally poor quality are added. Figure 4b shows this case. The sidelobe artifacts around the main beam, evident in the DSA image, have been removed. The measured values are 56.89, -10.7, 33.35, and 1.47, respectively. Figure 4c shows the performance of MSA-S. Three identical subarrays are used. The measured values are 58.34, -12.0, 30.55, and 1.23, respectively. Figure 4d shows the

performance of MSA-OS. The 330-element array was divided into three subarrays having 7 overlapped elements between adjacent subarrays. The first-two subarrays have 133 array elements and the third one has only 77 elements. Here, unequal size subarrays are used. The reason for unequal lengths is that the residual phase errors are not distributed uniformly across the array. The measured values show improvements in performance. They are 60.22, -12.4, 27.60, and 1.01, respectively. All these experimental results are listed in Table 2.

Figure 5 shows 2-D range-azimuth images of the power plant. Here, the sidelobe artifacts have been largely removed by using the MSA-OS. Thereby, the image is not significantly inferior to the high quality images.

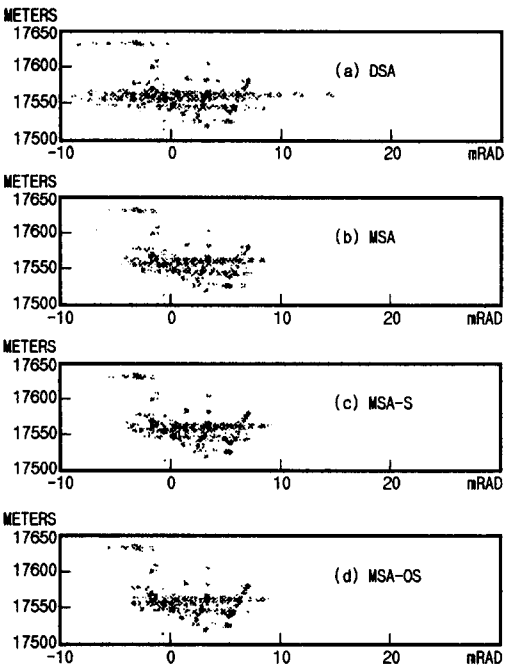

그림 5. 큰 분산 조건하에서 얻어진 Limerick 핵발전소의 range-azimuth 이미지
(a) DSA, (b) MSA, (c) MSA-S, (d) MSA-OS

Fig. 5. Range-azimuth images of Limerick nuclear power plant under high variance condition.
(a) DSA, (b) MSA, (c) MSA-S, (d) MSA-OS

표 2. 큰 분산 조건하에서의 dominant scatterer류의 알고리듬의 비교

Table 2. Comparison of dominant scatterer class of algorithms under high variance condition.

ABF algorithm	DSA	MSA	MSA-S	MSA-OS
Figure 4	a	b	c	c
σ^2_{NA} of bins	0.23 - -	0.23 0.20 0.21	0.23 0.20 0.21	0.23 0.20 0.21
Max amplitude	51.08	56.89	58.34	60.22
PSL (dB)	-6.9	-10.7	-12.0	-12.4
rms phase errors in degrees	46.74	33.35	30.55	27.60
$\triangle G$ (dB)	2.89	1.47	1.23	1.01

3. Image correlations

It is interesting to make a comparison by using the image correlation coefficient in (12). The best of the eight images is Figure 3d, as determined by residual *rms* phase data. Using it as the reference image, its correlations with Figures 3a-3c and 5a-5d are 0.97, 0.98, 0.99, 0.86, 0.91, 0.93, and 0.94, respectively. In [9], it is shown that a correlation coefficient of 0.9 or greater indicates satisfactory image formation. Based on this criterion, the DSA image (Figure 5a) fails while the MSA images (Figures 5b-5d) are satisfactory. Further, the MSA-OS performs the best.

V. Conclusions

We proposed a model of single point target embedded in clutter to define criteria to select the best ABF algorithm for high-resolution microwave imaging systems. Experimental data were used to compare the performance of the four ABF algorithms. When high quality ABF source is available ($\sigma^2_{NA} \leq 0.12$), the simple DSA is selected and there is no reason to resort to more complicated algorithms. When no high quality ABF source is found ($0.12 < \sigma^2_{NA} \leq 0.25$), the MSA-OS is selected for self-calibrating the large distorted phased array.

Acknowledgement

※ This paper is supported in part by Kongju National University research fund.

참 고 문 헌

[1] B.D. Steinberg, "Radar Imaging from a Distorted Array: the Radio Camera Algorithm and Experiment," IEEE Transactions on Antennas and propagation, vol. 29, no. 5, pp. 740-748, Sep. 1981.

[2] Currie, N.C. *et al.*, *Principles and Applications of Millimeter-Wave Radar*, Artech House, Norwood, MA, 1987.

[3] M.W. Long, *Radar Reflectivity of Land and Sea*, Artech House, Norwood, MA, 1983.

[4] B.D. Steinberg, *Microwave Imaging with Large Antenna Arrays:Radio Camera Principles and Techniques*, John Wiley and Sons, New York, 1983.

[5] E.H. Attia, "Self-Cohering Airborne Distributed Arrays Using the Robust Minimum Variance Algorithm," IEEE AP-S International Symposium, Antennas and Propagation, Phil- adelphia, PA, USA, vol. 2, pp. 603-606, June 1986.

[6] B. Kang, H.M. Subbaram, and B.D. Steinberg, "Improved Adaptive Beamforming Target for Self- Calibrating a Distorted Phased Array," IEEE Trans. on Antennas and Propagation, vol. 38, no. 2, pp. 186-194, 1990.

[7] B. Kang, B.D. Steinberg, and S.B. Kesler, "Improved Beamforming Target using Subarray Processing," Benjamin Franklin 8th Annual Symposium, "Advances in Antenna and Microwave Technology," IEEE AP/MTTS Philadelphia Section, pp. 52-53, Mar. 1990.

[8] E.H. Attia and B.D. Steinberg, "Self-Cohering Large Antenna Arrays Using the Spatial Correlation Properties of Radar Clutter," IEEE Transactions on Antennas and Propagation, vol, 37, no. 1, pp. 30-38, Jan. 1989.

[9] B.D. Steinberg, "A Theory of the Effect of Hard Limiting and Other Distortions Upon the Quality of Microwave Images," IEEE Trans. on Acoustics, Speech, and Signal Processing, vol. 35, no. 10, pp. 1462-1472, Oct. 1987.

[10] B. Kang and S. Park, "Target-to-Clutter Ratio as a Measure of Beamformer Quality," 대한전자공학회, 하계종합학술대회논문집, 제20권, 제1호, pp. 187-190, 6월, 1997

[11] J. Halat, "A Survey of Image-Embedded Passive Beamforming Sources for a Radio Camera," Master Thesis, University of Pennsylvania, Dec. 1985.

저 자 소 개

姜 鳳 淳(正會員) 第 34卷 D編 第 10號 參照

朴 成 鈞(正會員)

1962년 1월4일생. 1985년 2월 연세대 전자공학과 졸업(공학사). 1987년 2월 연세대 전자공학과 초고주파 전공(공학석사). 1987년 4월-1989년 8월 삼성전자 정보통신연구소 연구원. 1994년 2월 연세대 전자공학과 초고주파 전공(공학박사). 1994년 4월-1994년 8월 전자통신연구소 박사후 연수과정. 1994년 9월-현재 공주대학교 정보통신공학과 조교수 재직. 주관심분야는 이동통신 시스템 설계, 마이크로파 소자설계, 전파전파, fiber-optic link 시스템 등